

PAPER

[View Article Online](#)
[View Journal](#) | [View Issue](#)Cite this: *J. Mater. Chem. A*, 2025, **13**, 6663 α and γ mixed-phase Ga_2O_3 as a photocatalyst for CO_2 reduction with water: mechanism and the role of each phaseNaoto Ota,^a Yukie Takashiro,^a Muneaki Yamamoto,^b Tetsuo Tanabe^a and Tomoko Yoshida^{*ab}

Gallium oxides (Ga_2O_3) with mixed phases of α/β , β/γ , and α/γ are known to show high catalytic activity for the photoreduction of CO_2 with water to produce CO , H_2 and O_2 . However, the roles of each phase and phase mixing in the photocatalytic CO_2 reduction have not been well understood. In this study, we have synthesized α/γ mixed-phase Ga_2O_3 with controlled mixing ratios and examined their catalytic activity in the photoreduction of CO_2 with water. The catalytic activity or the production rates of H_2 and CO appreciably changed with the γ/α mixing ratio. The H_2 formation dominated on the α -phase, while the CO production increased with increasing the γ -phase content and attained the maximum for a γ -content of 40%. Above 60%, both the H_2 and CO production rates significantly decreased to the similar rates of the pure γ -phase. TEM observations of the mixed-phase Ga_2O_3 revealed the coexistence of spheroid type α - Ga_2O_3 particles with smaller polyhedral type γ - Ga_2O_3 which was not well crystallized to show a large surface area. In the α/γ mixed-phase Ga_2O_3 , γ - Ga_2O_3 was embedded in α - Ga_2O_3 with γ -phase contents less than 40%, while γ - Ga_2O_3 covered α - Ga_2O_3 above 60%. Considering that the H_2 and CO production rates change with the γ/α mixing ratio, we have revealed a reaction mechanism of CO production that some of the H produced on the α phase by water splitting is used to reduce CO_2 adsorbed on the γ -phase which has a much larger specific surface area than that of the α -phase but less catalytic activity than the α -phase.

Received 2nd December 2024
Accepted 20th January 2025

DOI: 10.1039/d4ta08531k

rsc.li/materials-a

Introduction

Gallium oxides (Ga_2O_3) have been attracting large interest as photocatalysts for water splitting, CO_2 reduction with water, CO_2 conversion into green fuels/chemicals, and degradation of pollutant chemicals.¹ In most studies of the CO_2 reduction with water using Ga_2O_3 as a photocatalyst, Ag or some metal oxides have been used as cocatalysts or dopants.^{2–6} Recently it has been reported that Ga_2O_3 works well as the photocatalyst for the CO_2 reduction without cocatalysts.^{7–12} Ga_2O_3 exhibits six different crystalline phases of α , β , γ , δ , ϵ , and κ , and a significant increase of the catalytic activity is reported with using mixed-phase Ga_2O_3 , for example, α/β mixed phases, γ/β mixed phases, γ/β phases + GaOOH , and GaOOH/α -phase.^{9–12} Aoki *et al.* have indicated that on α - Ga_2O_3 , photocatalytic water splitting dominates and the resulting hydrogen is used for CO_2

reduction.^{9,12} However, the effects of phase mixing or mechanism of enhancing the catalytic activity are not well known.

In this work, we have synthesized Ga_2O_3 consisting of the mixed phase of α and γ with different mixing ratios in order to investigate the roles of each phase in the photocatalytic CO_2 reduction and the mechanism of the enhancement of its catalytic activity. For the synthesis of α/γ mixed-phase Ga_2O_3 , a previously reported method by Li *et al.* was employed in which GaOOH and $\text{Ga}(\text{OH})_3$ were used as precursors of α - Ga_2O_3 and γ - Ga_2O_3 , respectively.¹³ Controlling preparation conditions carefully, we have succeeded in synthesizing the mixed-phase Ga_2O_3 with controlled mixing ratios for the first time and the mixing ratios of α/γ phases in the synthesized mixed-phase Ga_2O_3 were determined by XAFS analyses.

The synthesized mixed-phase Ga_2O_3 was subjected to photocatalytic CO_2 reduction with water as the photocatalyst. The production rates of H_2 and CO , major products of the CO_2 reduction, were analyzed in terms of the α/γ mixing ratio, specific surface area, grain (crystalline) size, particle size and morphology. The analysis leads us to conclude that the α -phase is quite effective for water splitting and the H produced by the water splitting reduces CO_2 dominantly adsorbed on the γ -phase. Accordingly, the maximum CO production rate appeared for the sample containing 40% γ -phase with a morphology of

^aDepartment of Applied Chemistry and Bioengineering, Graduate School of Engineering, Osaka Metropolitan University, Sugimoto 3-3-138, Sumiyoshi-ku, Osaka 558-8585, Japan

^bDepartment of Energy Engineering, Graduate School of Engineering, Nagoya University, Furo-cho, Chikusa-ku, Nagoya 464-8603, Japan. E-mail: tyoshida@energy.nagoya-u.ac.jp; Tel: +81-52-789-5935



small γ -phase grains embedded in a little larger α -phase particle.

Experimental

Preparation of photocatalyst samples

Photocatalyst samples of α/γ mixed-phase Ga_2O_3 were prepared by the following way. At first, the mixture of GaOOH and $\text{Ga}(\text{OH})_3$ was prepared by the impregnation method and the mixture was calcined to convert GaOOH and $\text{Ga}(\text{OH})_3$ to α - Ga_2O_3 and γ - Ga_2O_3 , respectively as reported by Li *et al.*, T. Sato *et al.* and Y. Hou *et al.*^{13–15} A fixed amount of $\text{Ga}(\text{NO}_3)_3 \cdot 8\text{H}_2\text{O}$ (KISHIDA Chemical Corporation, purity 99%) was dissolved into distilled water or ethanol and stirred for 1 hour. Then 28 mol% NH_3 aq. (FUJIFILM Wako Pure Chemical Corporation) solution was added in drops keeping constant pH. The deposits consisted of GaOOH and $\text{Ga}(\text{OH})_3$ and their mixing ratio was controlled by changing the stirring time and pH. Then the deposits were rinsed with distilled water, dried at 60 °C for a specified time, and calcined at 673 K in air for 4 hours resulting in the α/γ mixed-phase Ga_2O_3 . Detailed conditions for sample preparation are given in Table 1.

Characterization

Prepared α/γ mixed-phase Ga_2O_3 samples were characterized by X-ray diffraction analysis (XRD), scanning electron microscopy (SEM), transmission electron microscopy (TEM), specific surface area measurements, UV-vis diffuse reflection spectroscopy, and X-ray Absorption Fine Structure (XAFS) analysis. XRD patterns were recorded using a MiniFlex 600 instrument (Rigaku) at a voltage of 40 kV and current of 15 mA with $\text{Cu K}\alpha$ as the radiation source. The XRD patterns were collected at 20–80° in the 2θ angle scan. The 2θ scan step was 0.02° and the angle scanning rate of an X-ray detector was 10° min^{−1}. SEM

images were observed using a field emission scanning electron microscope (FE-SEM, JSM-6500F, JEOL Ltd) with a back-scattered electron mode under an acceleration voltage of 15 kV. TEM images were observed using a transmission electron microscope (JEM-2100Plus, JEOL Ltd) under an acceleration voltage of 200 kV. Specific surface areas (SSA) of all samples were measured by the BET method with a MonosorbTM instrument (Quantachrome). Before the BET measurements, each sample was heated at 573 K for 3 h under a nitrogen atmosphere. UV-vis spectra were obtained using a UV-visible near-infrared absorbance photometer (V-670, JASCO) with the diffuse reflection method using Ba_2SO_4 as the reference. The spectra were collected in the wavelength range of 190–850 nm. Ga K-edge XAFS measurements were performed at the Aichi Synchrotron Radiation Center BL5S1 or BL11S2 by the transmission method with using $\text{Si}(111)$ double crystals, and the ionization chambers were filled with 90% N_2 and 10% Ar for incident X-rays (I_0) and 70% N_2 and 30% Ar for transmitted X-rays (I).

Photocatalytic reduction of CO_2 with water

Photocatalytic CO_2 reduction with H_2O under UV light irradiation was performed using the sample of 0.1 g dispersed in an aqueous solution of 0.5 M NaHCO_3 set in a fixed-bed flow quartz reactor cell under CO_2 gas flow. The UV light given by a Xe lamp through the UV cold mirror was illuminated with the light intensity of 40 mW cm^{−2} at 254 ± 10 nm. CO_2 gas was flowed into the cell with a flow rate of 3 mL min^{−1}. The inside of the cell was stirred with a magnetic stirrer during the reaction. The reaction products (H_2 , O_2 and CO) were analyzed quantitatively using a gas chromatograph equipped with a thermal conductivity detector every one hour up to five hours or longer to confirm the steady state production rates.

Table 1 Conditions for the synthesis and results of characterization for α - Ga_2O_3 , α/γ - Ga_2O_3 and γ - Ga_2O_3

Preparation condition	Sample number																		
	1	2	3	4	5	6	7	8	9	10	11	12	13	14	15	16	17	18	19
γ phase concentration ^b (%)	0	0	3	4	5	7	15	19	24	40	50	56	58	61	63	79	80	92	100
Prepared Ga concentration (M)	0.1	0.05	0.10	0.1	0.1	0.1	0.15	0.05	0.1	0.1	0.2	0.1	0.1	0.1	0.1	0.1	0.2	0.2	0.1
Solvents	H_2O	H_2O	H_2O	H_2O	H_2O	H_2O	H_2O	H_2O	H_2O	H_2O	H_2O	H_2O	H_2O	H_2O	H_2O	H_2O	H_2O	H_2O	EtOH
Volume (mL)	100	100	100	100	100	100	100	200	100	100	100	100	100	100	100	100	50	50	100
Cover	×	○	○	○	○	○	○	○	○	×	○	○	×	○	○	○	○	○	○
Temperature (°C)	50	50	50	50	50	50	50	50	50	50	50	50	50	50	0	0	0	50	0
pH	9	9	9	8	9	9	9	9	9	9	9	10	9	9	10	10	12	9	10
Stirring time (h)	3	1	5	1	3	1	1	1	1	5	1	1	1	0	0	0	0	1	0
Drying temperature (°C)	60	60	60	60	60	60	60	60	60	60	60	60	60	60	25	25	25	60	25
Drying time (h)	24	15	24	15	24	15	15	15	24	24	15	15	24	15	1	15	15	15	15
Specific surface area (m ² g ^{−1})	42.79	38.54	39.09	46.33	36.12	44.17	51.46	62.35	59.49	45.93	68.75	64.5	82.91	94.27	72.3	81.58	106.15	91.36	129.09
Crystallite size of the α phase ^a	54.5	55	57	63.5	59.5	52.4	43.9	61.4	54.3	40.7	36.7	37.4	35.4	31.6	31.7	32.7	28.8	31.5	

^a Determined by XAFS analysis with the Ga K-edge. ^b Determined by XRD analysis using the (110) diffraction of α - Ga_2O_3 .



Results

Characterization

Fig. 1(a) and (b) show the XRD patterns of some samples before and after calcination, respectively. Before the calcination, sample 1 and sample 19 exhibited the single phase of GaOOH and Ga(OH)₃, respectively, and the other samples their mixtures. After the calcination, sample 1 (GaOOH) and sample 19 (Ga(OH)₃) turned to be the fully α -phase (α -Ga₂O₃) and γ -phase (γ -Ga₂O₃), respectively, while the other samples turned to be the mixture of the α -phase and the γ -phase (referred as to α/γ -Ga₂O₃ samples).

The XRD peaks of the α -phase were sharp enough to determine their crystallite sizes in the α/γ -Ga₂O₃ samples from the full width at half maximum (FWHM) of the (110) peak of the α -phase. The determined crystallite sizes are given in the bottom column of Table 1 and plotted against γ phase contents in Fig. 2. As seen in the figure, the size decreased almost linearly with increasing the γ phase content. On the other hand, the XRD peaks of the γ -phases were very broad indicating poor crystallization. This makes it impossible to determine the crystallite sizes of the γ -phase from the FWHM. It also makes it hard to determine the mixing ratio of α/γ phases (α/γ phase

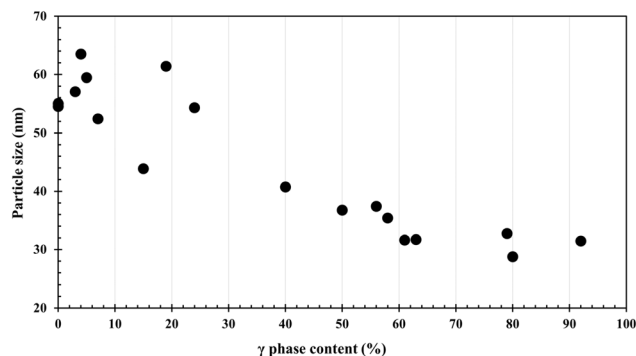


Fig. 2 Changes of crystallite size determined by XRD analysis using the (110) diffraction of α -Ga₂O₃ with the contents of the γ phase.

ratio) in the samples with the X-ray peak intensity ratio of both the phases. Therefore, the α/γ phase ratios represented as the γ contents in the α/γ -Ga₂O₃ samples were determined with the quantitative structural analysis using XANES and EXAFS as follows.

In Fig. 3(a) are compared three Ga K-edge XANES for α -Ga₂O₃, γ -Ga₂O₃ and sample 10 (α/γ -Ga₂O₃) with the inset of an enlarged one. Quantitative structural analysis using XANES is

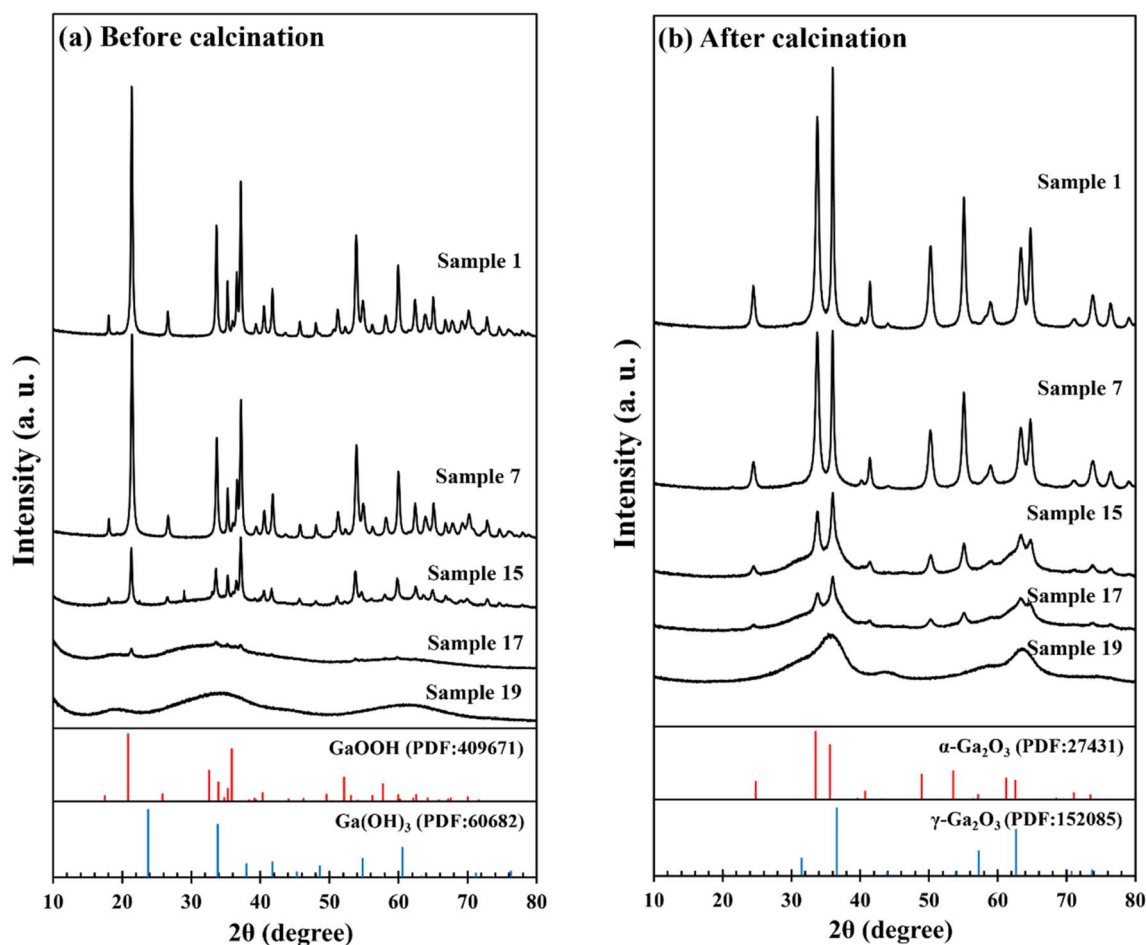


Fig. 1 XRD patterns of samples (a) before and (b) after calcination.



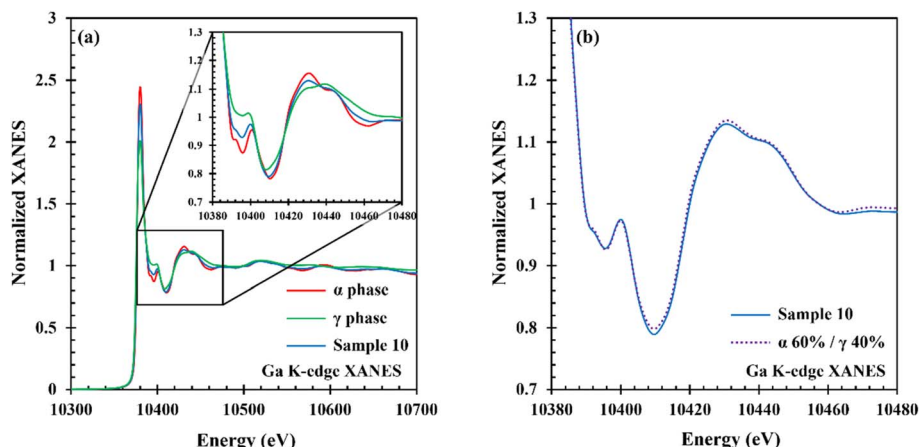


Fig. 3 (a) Ga K-edge XANES spectra of α -Ga₂O₃, γ -Ga₂O₃, and α/γ -Ga₂O₃ samples with enlarged views. (b) Least square fitting to the observed spectra with a linear combination of the spectra of α -Ga₂O₃ (60%) and γ -Ga₂O₃ (40%).

usually performed with microstructures that appeared at higher energy than the XANES absorption edge. As seen in Fig. 3(a), the difference in crystalline phases is apparent. Assuming the fine structures of α -Ga₂O₃ and γ -Ga₂O₃ were kept in α/γ -Ga₂O₃ samples, the fine structure of the α/γ -Ga₂O₃ sample was reproduced by the linear combination of those of α -Ga₂O₃ and γ -Ga₂O₃ with changing the combination ratio. The best fit result for sample 10 in Fig. 3(a) is given in Fig. 3(b) as the superposition of the observed one and reproduced one with a combination ratio of 60% α -Ga₂O₃ and 40% γ -Ga₂O₃. The reproduction by the linear combination was quite well with an error of a few %. Similar analysis was done for EXAFS as shown in Fig. 4. Fig. 4(a) is those for α -Ga₂O₃, γ -Ga₂O₃, and sample 10 and Fig. 4(b) compares the linear combination of EXAFS of α -Ga₂O₃ and γ -Ga₂O₃ with EXAFS of sample 10. The EXAFS analysis gave a quite similar α/γ mixing ratio to the XANES analysis. Thus, the determined mixing ratios of α -Ga₂O₃ and γ -Ga₂O₃ (α/γ mixing ratio) in all samples are given in the top column of Table 1 as the content of the γ -phase (%).

The results of BET specific surface area measurements are given Table 1 in the second line from the bottom, and are

plotted against the γ -phase contents determined by the XANES analysis in Fig. 5. It is interesting to note that the specific surface area increases roughly linearly with the γ -phase content.

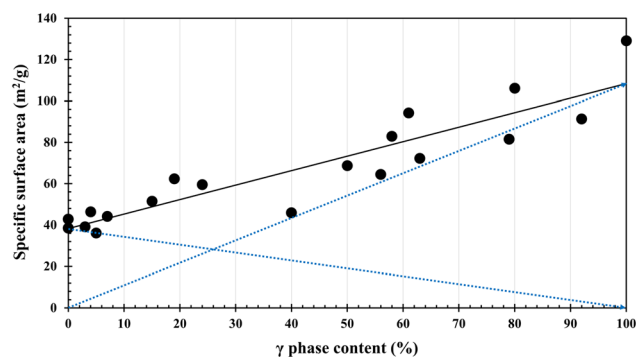


Fig. 5 Changes of BET specific surface area with γ phase contents. Lines are for guide to the eye. As seen in two dotted line lines, the surface areas are well represented with the linear combination of the surface areas of each phase.

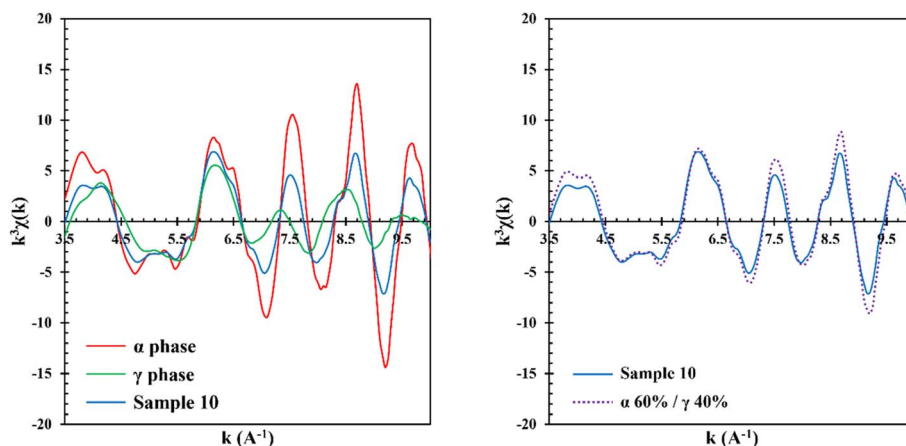


Fig. 4 (Right) Ga K-edge EXAFS spectra of α -Ga₂O₃, γ -Ga₂O₃ and α/γ -Ga₂O₃ samples. (Left) Least square fitting to the observed spectra with a linear combination of the spectra of α -Ga₂O₃ (60%) and γ -Ga₂O₃ (40%).



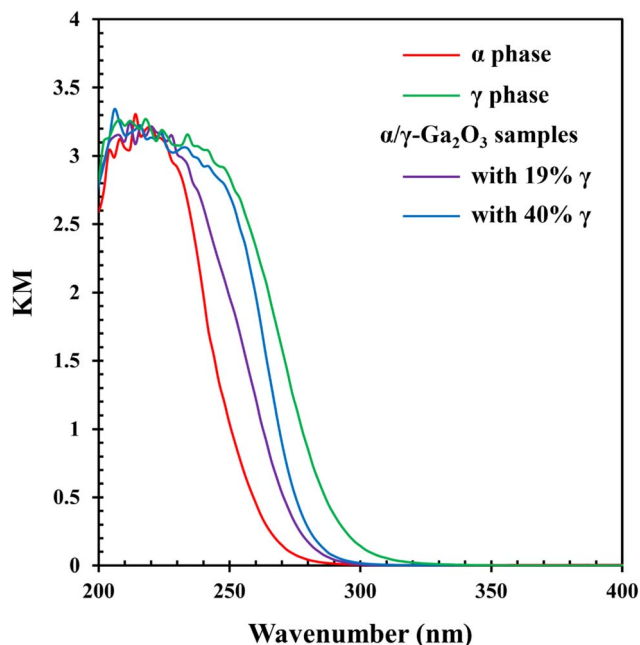


Fig. 6 UV-vis spectra of α -Ga₂O₃, γ -Ga₂O₃ and α/γ -Ga₂O₃ samples with γ phase contents of 19% and 40%.

Fig. 6 shows the UV-vis spectra of α -Ga₂O₃, γ -Ga₂O₃ and α/γ -Ga₂O₃ samples. Although their band gap widths decreased with increasing γ -phase contents, no significant change appeared. This is consistent with the smooth changes of the BET surface area in Fig. 5.

Morphology

Fig. 7 shows the SEM images of (a) α -Ga₂O₃, (b) sample 10 (α/γ -Ga₂O₃) and (c) γ -Ga₂O₃. α -Ga₂O₃ consists of spheroid type particles uniformly with a length of nearly 1 μ m. In the α/γ -Ga₂O₃ samples, with increasing the γ -phase contents, their particle sizes gradually increased accompanying structure disorder or surface roughening. For higher γ -phase containing samples, the particle shape changed to polygons with random sizes. Fig. 8 shows the TEM images of (a) α -Ga₂O₃, (b) sample 10 (α/γ -Ga₂O₃) and (c) γ -Ga₂O₃ respectively corresponding to Fig. 7. The images clearly show that every particle observed in SEM consisted of small crystallites. In α -Ga₂O₃ (Fig. 8(a)) spheroid type crystallites with a length of several tens of nm were

unidirectionally aligned, while those in γ -Ga₂O₃ (Fig. 8(c)) were polygons (or rather spherical) with sizes of less than 10 nm. The size of the spheroid type crystallite in the α phase is consistent with the particle sizes determined by the XRS analysis, ranging from 70 to 30 nm (see Table 1). The smaller crystallite size of the γ -phase well corresponds to its larger BET surface area. The α/γ -Ga₂O₃ sample (Fig. 8(b)) seems to be consisting of two different shaped particles of spheroids and polygons. To confirm this mixing of γ -phase and α -phase, the diffraction patterns of several localized areas in the particles of the α/γ -Ga₂O₃ sample were observed Fig. 8(d) and (e) are typical examples of the TEM image the particle and the diffraction pattern which consisted of diffraction spots assigned to (110) and (300) of the α -phase, and halo patterns to (331) and (731) of the γ -phase were appreciable.

These observations lead us to conclude that the α/γ -Ga₂O₃ samples consisted of two different types of fine particles; one is the spheroid type shaped and well crystallized α -Ga₂O₃ and the other is the polyhedron type and not well crystallized γ -Ga₂O₃. In addition, for the α/γ -Ga₂O₃ samples with lower γ -Ga₂O₃ contents, smaller polyhedrons of γ -Ga₂O₃ were embedded in the larger α -Ga₂O₃ spheroids, while for the higher γ -Ga₂O₃ contents the smaller α -Ga₂O₃ spheroids were surrounded by the polyhedrons of γ -Ga₂O₃.

Photocatalytic reduction of CO₂ with water

All photocatalytic experiments have been performed over 5 hours to confirm that the production rates of H₂, CO and O₂ became constant.

The dominant products of the photocatalytic reduction with water using the catalyst samples were H₂, CO and O₂. Their production rates satisfied the stoichiometry of $([H_2] + [CO])/[O_2] = 1$, where $[H_2]$, $[CO]$, and $[O_2]$ are the production rates of H₂, CO, and O₂, respectively. In Fig. 9 are plotted the production rates of H₂ and CO for all catalyst samples against the contents of the γ -phase. The CO production rates increased by increasing the γ -phase content up to 40% and then decreased. Over 60% the CO production rates became small without clear correlation with the γ -phase contents. The H₂ production rates were high for samples with lower γ -phase contents, while they were small for those samples with higher γ -phase contents over 60%. Both production rates seem differently depend on the γ -phase contents. However, as shown in Fig. 10 the ratios of the production rates of H₂ and CO are clearly correlated with the γ -

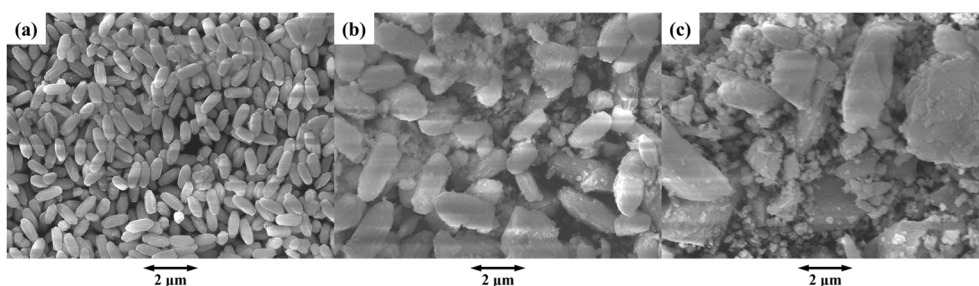


Fig. 7 SEM images of (a) α -Ga₂O₃, (b) α/γ -Ga₂O₃ with a γ phase content of 40% and (c) γ -Ga₂O₃.



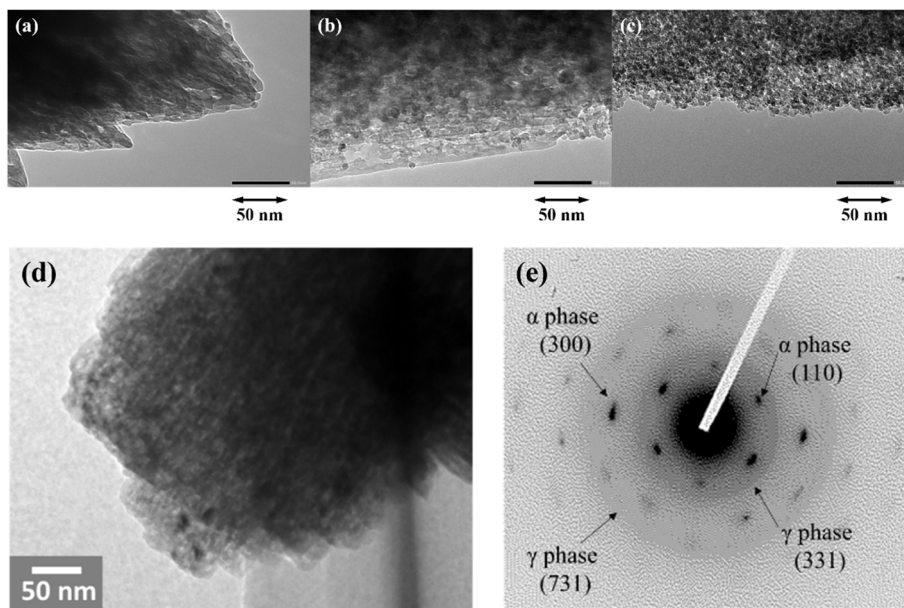


Fig. 8 TEM images of (a) α -Ga₂O₃, (b) α/γ -Ga₂O₃ with a γ phase content of 40% and (c) γ -Ga₂O₃, and (d) the enlarged image of a particle appeared in (b) and (e) its electron diffraction pattern.

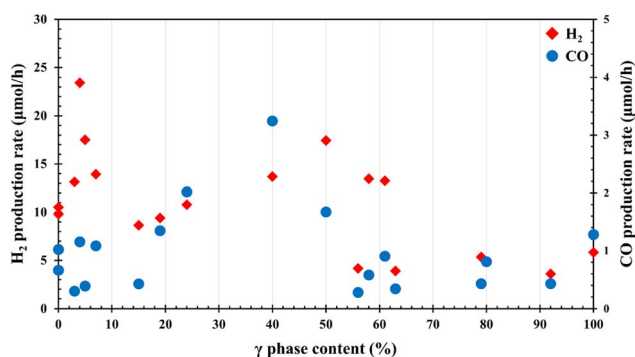


Fig. 9 Production rates of H₂ and CO plotted against the γ phase contents of the α/γ -Ga₂O₃ samples.

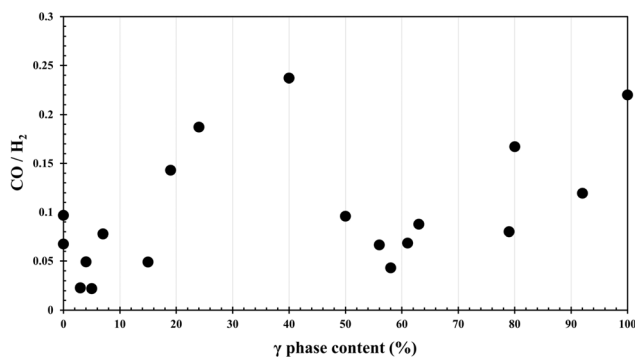


Fig. 10 Ratios of the production rates of CO and H₂ plotted against the γ phase contents of the α/γ -Ga₂O₃ samples.

phase contents. Furthermore, the figure suggests that the reaction mechanism changes in the samples with γ -phase

contents of below and above 60%. The reaction mechanism is discussed separately in the next section.

After the photocatalytic reduction, XRD and UV-vis of the samples showed no significant change except the new appearance of a small peak attributed to GaOOH in XRD.

Discussion

As seen in Fig. 5, BET surface areas of the α/γ Ga₂O₃ samples roughly linearly increased with the γ -phase contents and are well represented by the linear combination of those of the pure α -phase and pure γ -phase with the coefficient of each phase. This indicates that the BET surface areas of both the phases in the α/γ Ga₂O₃ samples were not influenced by the phase mixing. The observation of UV-vis also supports this. In addition, those of the α/γ Ga₂O₃ samples were dominated by the BET surface area of the γ -phase. This is because the γ -phase was not well crystallized or included various defects as indicated by its broad X-ray spectrum in Fig. 1 and the halo patterns of TEM diffraction in Fig. 8(e). In addition, the activity of the α/γ Ga₂O₃ samples with γ -phase contents more than 60% was weak similar to or even less than that of the pure γ -phase. The difference more clearly appeared in the ratio of the production rates of H₂ and to CO (see Fig. 10), indicating that the mechanism of CO₂ reduction was different between the samples containing the γ -phase less than 60% and higher ones.

In the following, discussed is the mechanism of higher activity of the samples containing the γ -phase less than 60%. As seen in Fig. 9, H₂ is mainly formed on the α -phase, while CO production increased by increasing the γ -phase content, reaching a maximum at about 40% γ -phase, and then decreasing despite the increase in the BET surface area. Considering redox type photocatalytic water splitting on the



Ga₂O₃ catalyst indicated in previous studies, the present results strongly suggest that the H produced on the α -phase by the water splitting is used to reduce the CO₂ adsorbed on the γ -phase, which has a large specific surface area.^{7–12} In the previous studies, we have confirmed the surface adsorption of CO₂ as carbonate forms on Ga₂O₃.^{11,16,17}

Based on this, we assume that some of the H produced on α - and γ -phases in the α/γ -Ga₂O₃ sample reduces CO₂ adsorbed on either the α - or γ -phase and estimate how CO₂ reduction rates change with the mixing ratio of α/γ -phases. Considering the

BET surface change given in Fig. 5, we have employed an additional assumption that H production rates on the α -phase and the γ -phase do not change with the mixing. Then CO production rates in the α/γ -Ga₂O₃ samples can be calculated as follows. The reaction rates of hydrogen and CO on the α and γ phases are set to be $v(\text{H}_2)_\alpha$ and $v(\text{CO})_\alpha$, and $v(\text{H}_2)_\gamma$ and $v(\text{CO})_\gamma$, respectively, which are given as observed experimental values for the α and γ single phase samples. Then the CO generation on the mixed phase samples can be divided into the following three contributions; (1) CO generation caused by hydrogen generated on the α phase, (2) CO generation caused by hydrogen generated on the γ phase, and (3) CO generation on the γ phase caused by hydrogen generated on the α phase with the efficiency of k .

Since the hydrogen production rate on each phase in a α/γ -Ga₂O₃ sample should be proportional to the respective content of the α - and γ -phases, the CO production rates for the above three contributions are given as $(1-x)v(\text{CO})_\alpha$, $xv(\text{CO})_\gamma$, and $k(1-x)v(\text{H}_2)_\alpha$, respectively. Here x is the content of the γ -phase. Then the total CO production rate in the α/γ -Ga₂O₃ samples is represented as

$$v(\text{CO})_{\text{total}} = (1-x)v(\text{CO})_\alpha + xv(\text{CO})_\gamma + k(x-x^2)(v(\text{H}_2)_\alpha) \quad (1)$$

In Fig. 11, eqn (4) with the adjustment of k to fit the experimental results is superposed on the experimentally obtained CO₂ production rates. Although the data are scattered, the model calculation fits well. And the third term of eqn (1) dominates in the total reaction rates. This means that the CO₂ reduction on the α/γ -Ga₂O₃ samples is dominated by the reaction that H produced on the α -phase is used to reduce CO₂ adsorbed on the γ -phase.

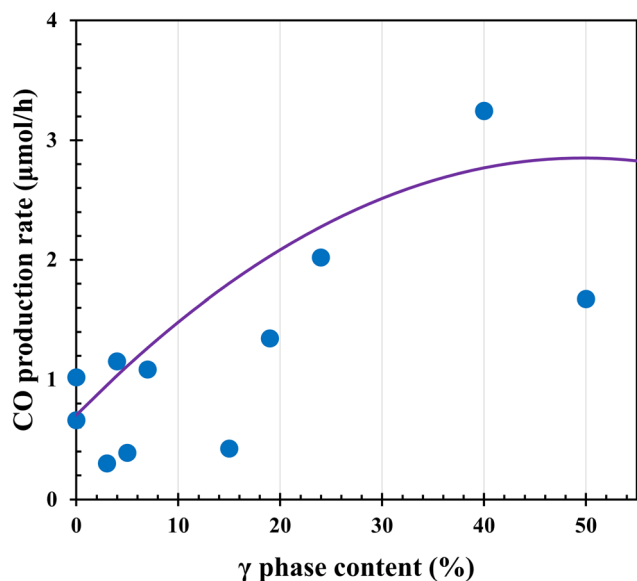
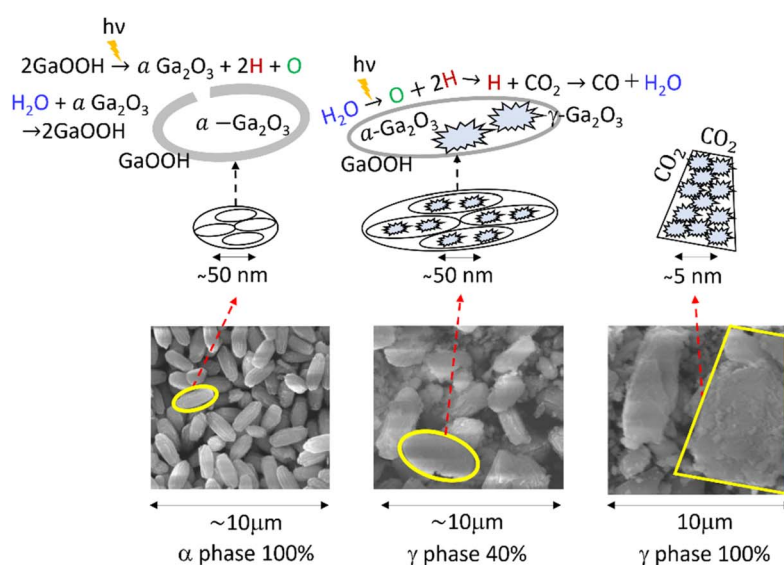


Fig. 11 Comparison of CO production rates estimated by eqn (4) with the observed ones for the α/γ Ga₂O₃ samples with a γ phase content up to 50%.



Schematic drawing of morphology of α/γ Ga₂O₃ photocatalysts and CO production mechanism

Fig. 12 Schematic drawing of the CO production mechanism on the α/γ -Ga₂O₃ samples and morphologies of α -Ga₂O₃, α/γ -Ga₂O₃ with the γ -concentration of 40% and γ -Ga₂O₃ (see text).

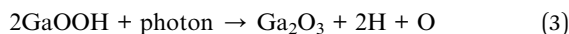


In the previous work, Aoki *et al.* indicated that photocatalytic water splitting on α -Ga₂O₃ proceeds through the following redox reactions of α -Ga₂O₃ and GaOOH.^{9,12}

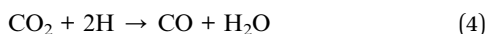
In water, the surface of α -Ga₂O₃ is oxyhydrized as,



and photo-irradiation reduces GaOOH producing H and O as,



Thus produced H reduces CO₂ as



In the present work, the formation of GaOOH was also observed in the XRD of the samples after use.

Considering all the above, the mechanism of the CO production on the mixed phase sample is schematically drawn as given in Fig. 12. From the morphology determined by XRD, SEM and TEM, the mixed phase samples consist of spheroid type α -Ga₂O₃ particles with smaller polyhedral type γ -Ga₂O₃ which was not well crystallized to show a large surface area and embedded in the α -Ga₂O₃ particles. Hydrogen is dominantly produced on the α -Ga₂O₃ particles thorough the redox of Ga₂O₃ and GaOOH and migrates to the γ -Ga₂O₃ particles embedded in the larger α -Ga₂O₃ particles to reduce CO₂ adsorbed on it.

In samples containing the γ -phase more than 60%, the particles of γ -Ga₂O₃ dominate to cover the minor α -Ga₂O₃ particles to inhibit oxyhydration of α -Ga₂O₃. Consequently, hydrogen production is suppressed resulting in less CO production. Although the oxyhydration of γ -Ga₂O₃ would be possible, the product is very likely Ga(OH)₃ which is the precursor of γ -Ga₂O₃ as seen in Fig. 1. The reduction of Ga(OH)₃ by photons would be possible



However, it requires major re-arrangement of Ga and O atoms, and the reaction would be harder to proceed. Accordingly, hydrogen production on the γ -phase is much less than that on the α -phase.

Conclusions

We have succeeded in synthesizing α/γ mixed-phase gallium oxides (α/γ -Ga₂O₃) with controlled α/γ mixing ratios by impregnation and calcination. The α/γ phase mixing ratios were determined quantitatively by XAFS structural analysis with the Ga K-edge. The prepared α/γ -Ga₂O₃ was used as the catalyst for the photoreduction of CO₂ with water. Although the specific surface areas of α/γ -Ga₂O₃ nearly linearly increased from 38 m² g⁻¹ of the pure α -phase to 130 m² g⁻¹ for the pure γ -phase, they did not correlate well with the catalytic activity or the production rates of H₂ and CO. Instead, the production rates of H₂ and CO appreciably changed with the mixing ratio. The H₂ formation dominated on the α -phase, while the CO production

increased with increasing the γ -phase content and attained the maximum for a γ -content of 40%. Above 60% both the H₂ and CO production rates decreased to the similar rates of the pure γ -phase much less than that of the pure α -phase. The ratio of the production rates of H₂ and CO also increased with increasing the γ -content to the maximum at a γ -content of 40%. Above 40%, it decreased taking a minimum and then increased again suggesting a different mechanism for α -dominated and γ -dominated α/γ -Ga₂O₃.

According to a reaction mechanism in the previous work, CO production in the photocatalytic CO₂ reduction with water on α -Ga₂O₃ catalysts proceeds thorough the reaction of adsorbed CO₂ with H produced by the water splitting. In analogy with this mechanism, we have assumed that some of the H produced on the α -phase reduces CO₂ adsorbed on the γ -phase and made a kinetic equation to give the CO production rate taking into account the H production rate on the α phase and CO production rates with the reaction of H produced on the α -phase and CO₂ adsorbed on the γ phase, and the contents of both the phases. The equation fits well to the observed relation of the CO production rates with the α/γ mixing ratio up to a γ content of 50%. This confirms the reaction mechanism that H produced on the α -phase reduces CO₂ adsorbed on the γ -phase.

TEM observations of α/γ -Ga₂O₃ revealed that the spheroid type α -Ga₂O₃ particles were coexisting with smaller polyhedral type γ -Ga₂O₃ which was not well crystalized to show a large surface area. In α/γ -Ga₂O₃ containing the γ -phase less than 40%, γ -Ga₂O₃ particles were embedded in the α -Ga₂O₃ particles, while in α/γ -Ga₂O₃ containing the γ -phase more than 60% γ -Ga₂O₃ particles covered α -Ga₂O₃ particles. These observations well correspond to the above reaction mechanism below 50% and similar activities with the γ -phase for above 60%.

Data availability

Raw data were generated at Osaka Metropolitan University. Derived data supporting the findings of this study are available from Tomoko Yoshida on request.

Conflicts of interest

The authors declare no conflict of interest.

References

- 1 Z. Huang, K. Teramura, H. Asakura, S. Hosokawa and T. Tanaka, *Curr. Opin. Chem. Eng.*, 2018, **20**, 114.
- 2 M. Yamamoto, T. Yoshida, N. Yamamoto, T. Nomoto, Y. Yamamoto, S. Yagi and H. Yoshida, *J. Mater. Chem. A*, 2015, **3**, 16810.
- 3 N. Yamamoto, T. Yoshida, S. Yagi, Z. Like, T. Mizutani, S. Ogawa, H. Nameki and H. Yoshida, *e-J. Surf. Sci. Nanotechnol.*, 2014, **12**, 263.
- 4 Y. Pan, Z. Sun, H. Cong, Y. Men, S. Xin, J. Song and S. Yu, *Nano Res.*, 2016, **9**, 1689.
- 5 S. Kikkawa, K. Teramura, H. Asakura, S. Hosokawa and T. Tanaka, *J. Phys. Chem. C*, 2018, **122**, 21132.



- 6 H. Yoon, J. Yang, S. Park, C. Rhee and Y. Sohn, *Appl. Surf. Sci.*, 2021, **536**, 147753.
- 7 P. Chen, K. Li, B. Lei, L. Chen, W. Cui, Y. Sun, W. Zhang, Y. Zhou and F. Dong, *ACS Appl. Mater. Interfaces*, 2021, **13**, 50975.
- 8 K. Sonoda, M. Yamamoto, T. Tanabe and T. Yoshida, *Appl. Surf. Sci.*, 2021, **542**, 148680.
- 9 T. Aoki, M. Yamamoto, T. Tanabe and T. Yoshida, *New J. Chem.*, 2022, **46**, 3207.
- 10 M. Akatsuka, Y. Kawaguchi, R. Itoh, A. Ozawa, M. Yamamoto, T. Tanabe and T. Yoshida, *Appl. Catal., B*, 2020, **262**, 118247.
- 11 Y. Kawaguchi, M. Yamamoto, A. Ozawa, Y. Kato and T. Yoshida, *Surf. Interface Anal.*, 2019, **51**, 79.
- 12 T. Aoki, K. Ichikawa, K. Sonoda, M. Yamamoto, T. Tanabe and T. Yoshida, *RSC Adv.*, 2022, **12**, 7164.
- 13 L. Li, W. Wei and M. Behrens, *Solid State Sci.*, 2012, **14**, 971.
- 14 T. Sato and T. Nakamura, *J. Chem. Technol. Biotechnol.*, 1982, **32**, 433.
- 15 Y. Hou, L. Wu, X. Wang, Z. Ding, Z. Li and X. Fu, *J. Catal.*, 2007, **250**, 12.
- 16 M. Yamamoto, S. Yagi and T. Yoshida, *Catal. Today*, 2018, **303**, 334.
- 17 M. Yamamoto, T. Yoshida, N. Yamamoto, H. Yoshida and S. Yagi, *e-J. Surf. Sci. Nanotechnol.*, 2014, **12**, 299.

